sp<sup>3</sup>-Functionalization of Single-Walled Carbon Nanotubes Creates Localized Spins

Sven-Hendrik Lohmann, <sup>1</sup> Kasidet Jing Trerayapiwat, <sup>2</sup> Jens Niklas, <sup>3</sup> Oleg G. Poluektov, <sup>3</sup> Sahar Sharifzadeh, <sup>2,4</sup> Xuedan Ma<sup>1,5\*</sup>

<sup>1</sup>Center for Nanoscale Materials, Argonne National Laboratory, Lemont, IL 60439, USA

<sup>2</sup>Department of Chemistry, Boston University, Boston, Massachusetts 02215, United States

<sup>3</sup>Chemical Sciences and Engineering Division, Argonne National Laboratory, Lemont, Illinois

60439, USA

<sup>4</sup>Division of Materials Science and Engineering and Department of Electrical and Computer

Engineering, Boston University, Boston, Massachusetts 02215, United States

<sup>5</sup>Consortium for Advanced Science and Engineering, University of Chicago, Chicago, Illinois

60637, United States

#### **ABSTRACT**

Chemical functionalization-introduced  $sp^3$  quantum defects in single-walled carbon nanotubes (SWCNTs) have shown compelling optical properties for their potential applications in quantum information science and bioimaging. Here, we utilize temperature- and power-dependent electron spin resonance measurements to study the fundamental spin properties of SWCNTs functionalized with well-controlled densities of  $sp^3$  quantum defects. Signatures of isolated spins that are highly localized at the  $sp^3$  defect sites are observed, which we further confirm with density functional theory calculations. Applying temperature-dependent linewidth analysis and power-saturation

measurements, we estimate the spin-lattice relaxation time  $T_1$  and spin dephasing time  $T_2$  to be around 9 µs and 40 ns, respectively. These findings of the localized spin states that are highly associated with the  $sp^3$  quantum defects not only deepen our understanding of the molecular structures of the quantum defects, but could have strong implications for their applications in quantum information science.

KEYWORDS: single-walled carbon nanotubes, electron spin resonance,  $sp^3$  quantum defects, spin-lattice relaxation time, spin coherence time

## **INTRODUCTION**

Controlled chemical functionalization is an effective approach to create optically-active quantum defects in semiconductor single-walled carbon nanotubes (SWCNTs).<sup>1-4</sup> By introducing a deeplying electronic state within the bandgap, diffusive excitons that would originally have been consumed at quenching sites become captured by the quantum defects, allowing effective recombination to occur.<sup>5-9</sup> Through this approach, a significant enhancement in the photoluminescence quantum yield has been demonstrated.<sup>1, 2, 9</sup> The localized excitonic state also diminishes the occurrence of multiexciton emission,<sup>10-12</sup> and enables the observation of single photon emission from the defect sites at room temperature.<sup>13-15</sup> Due to their mechanical stability and compatibility with microfabrication techniques, chemically-functionalized SWCNTs can be readily integrated into photonic and optoelectronic devices.<sup>16-22</sup>

SWCNTs also support fascinating spin properties that may facilitate their applications for spinqubits<sup>23, 24</sup> and spintronics.<sup>25, 26</sup> Due to the weak spin-orbit coupling and the absence of nuclear spins in the dominant <sup>12</sup>C isotope, SWCNTs are predicted to support long spin coherence times.<sup>27, 28</sup> Coupling of spin states in SWCNTs to valley,<sup>24, 29</sup> mechanical,<sup>30, 31</sup> and microwave photonic<sup>32, 33</sup> degrees of freedom has been proposed as enabling techniques for spin qubit manipulation and detection. Another intriguing approach for spin manipulation is to leverage spin-photon interactions,<sup>34-36</sup> which could provide means for improved manipulation time and direct integration with photonic networks. The realization of this scheme, however, relies heavily on the confinement of electron spins to form a quantum two-level system, a property that is extraneous to one-dimensional SWCNTs.<sup>26</sup>

Here, we investigate the spin properties, including their dynamics and wave function localization, in (6,5)-SWCNTs. Our temperature- and power-dependent electron spin resonance (ESR) studies reveal a striking difference between pristine SWCNTs and those chemically functionalized with  $sp^3$  quantum defects. While negligible ESR response is observed for the pristine SWCNTs, signatures of localized spins isolated from each other can be detected in the functionalized SWCNTs. Our comparison of the quantum defect and localized spin densities suggests the quantum defect-related origin of the spins, which is further confirmed by our density functional theory calculations. The spin-lattice relaxation time  $T_1$  and spin coherence time  $T_2$  of the localized spins are estimated to be around 9  $\mu$ s and 40 ns, respectively. These findings are highly relevant to the understanding of spin-photon interactions in SWCNTs and may expand their potential applications in quantum information science.

## RESULTS AND DISCUSSION

We utilize the diazonium salt doping method to introduce  $sp^3$  quantum defects onto the sidewalls of (6,5)-SWCNTs (see Methods for the detailed doping procedure).<sup>2,37</sup> The doping progress and the corresponding quantum defect density can be controlled by monitoring the photoluminescence (PL) spectra of the SWCNTs. Fig. 1b shows a representative PL spectrum of (6,5)-SWCNTs chemically functionalized by 4-nitrobenzenediazonium tetrafluoroborate (NO<sub>2</sub>-Dz, sketch shown in Fig. 1a). The introduced  $sp^3$  quantum defects manifest themselves as deep trapping states ( $E_{11}^*$ ) giving rise to a bright PL peak that is red-shifted by around 170 nm from the original  $E_{11}$  peak in the pristine SWCNTs. To ensure sufficient signal-to-noise ratio in the ESR measurements, the

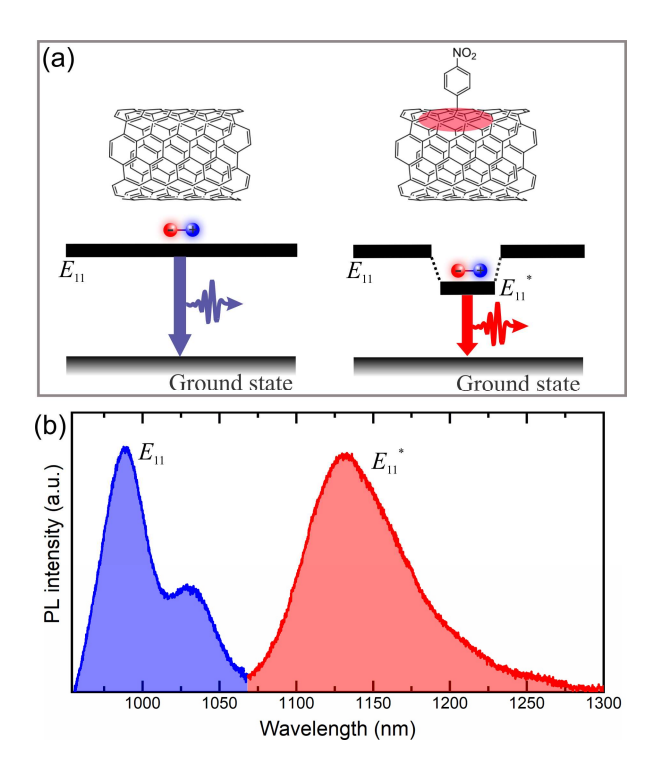


Figure 1. (a) The structures of a pristine (left) and 4-nitrobenzenediazonium tetrafluoroborate functionalized (NO<sub>2</sub>-Dz-) SWCNTs (right) together with their corresponding band-edge energy levels. (b) A representative photoluminescence spectrum of (6,5) NO<sub>2</sub>-Dz-SWCNTs, with the  $E_{11}$  emission marked blue and the  $sp^3$  defect-induced  $E_{11}^*$  emission marked red.

quantum defect density is optimized to be sufficiently high but without causing quenching of the SWCNT PL.<sup>2, 6</sup>

To investigate the spin properties of the SWCNTs, we carry out ESR measurements of pristine and chemically functionalized SWNCTs. ESR is a spectroscopic technique for investigating unpaired electrons in systems such as free radicals,<sup>38</sup> conduction electrons,<sup>39</sup> and transition metals. 40 Due to the tremendous amount of research interest in the spin properties of SWCNTs. 25, <sup>27, 29, 30, 32, 41</sup> there has been considerable effort devoted to the ESR studies of pristine SWCNTs. However, controversy remains regarding the origin of the observed ESR signals 42-47 and the related interpretation of the lineshape and magnetic susceptibility. 42, 44, 45, 47, 48 Factors such as the purifying procedure, 46 growth method, 49 and physisorption of gas molecules 47 further complicate the investigation of the underlying physics. In our study, purified single-chirality (6,5)-SWCNTs are used, which helps rule out contributions from catalyst particles and carbon impurities. Fig. 2a shows a representative continuous wave (cw) X-band ESR spectrum from pristine SWCNTs where no apparent signal can be observed. This finding is consistent with previous ESR studies on purified SWCNTs, 46, 50 showing that the intrinsic ESR response of conduction electrons in SWCNTs is too weak to be detected at X-band and modest magnetic fields. One potential explanation is that the one-dimensional nature of the itinerant electrons in SWCNTs promotes a Luttinger liquid state, 51,52 which leads to a significant line broadening in the ESR signal (can reach up to 1000 G at 4 K), making it too weak to be detected. 50,53 Consideration of spin-orbit coupling in SWCNTs yields a similar conclusion:<sup>46</sup> Based on previous measurements<sup>54</sup> and theoretical calculations, 55 the spin-orbit coupling strength for the (6,5)-SWCNTs used in this study could be estimated to be around 250 GHz, which is much higher than the X-band (9.5 GHz) in our ESR

measurement. The absence of ESR response from our pristine SWCNTs also indicates the high quality of the samples with minimal defects and unpaired electrons. 44,50

More importantly, these measurements of the pristine SWCNTs serve as reliable references for our investigation of the functionalized SWCNTs. By keeping the concentrations of the pristine and functionalized samples similar, direct comparison of the relative spin densities in the different types of samples can be made. Fig. 2b shows an ESR spectrum obtained from NO<sub>2</sub>-Dz-doped (6,5)-SWCNTs at 10 K, which shows strikingly different features compared to the spectra of the pristine SWCNTs. It consists of a single narrow line with a Landé g-factor of  $2.0037 \pm 0.0003$ , the value of which exhibits little temperature dependence. No broad ferromagnetic signal is observed, attesting that majority of the catalyst particles have been removed such that their concentrations are below the ESR detection limit.<sup>44,56</sup> The distinct ESR spectra of the pristine and functionalized

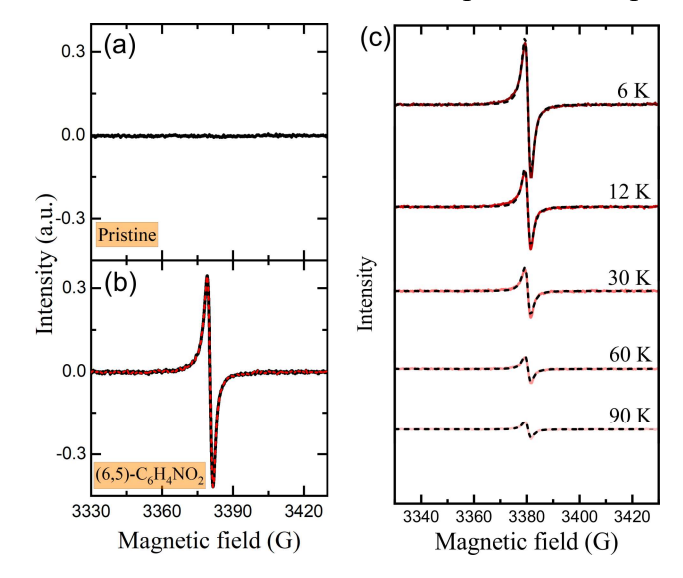


Figure 2. (a) A representative cw X-band ESR spectrum of pristine (6,5)-SWCNTs at 10 K and microwave power of 0.5 mW. (b) A representative cw X-band ESR spectrum (black) of NO<sub>2</sub>-Dz-doped SWCNTs at 10 K and microwave power of 0.5 mW, together with a Dysonian fitting curve (red). (c) Representative temperature-dependent cw X-band ESR spectra of NO<sub>2</sub>-Dz-doped SWCNTs at the power of 0.5 mW with their corresponding Dysonian fitting curves.

SWCNTs infer the generation of unpaired electrons in the functionalized SWCNTs through the doping process. We note that our measurements of 4-nitrobenzenediazonium tetrafluoroborate solutions under similar experimental conditions yield no apparent ESR signals (Fig. S1), which precludes the possibility that the ESR signals observed in Fig. 2b and 2c originate from residual diazonium salts in the SWCNT solutions.

The intensity of the ESR signal from the functionalized SWCNTs shows a clear temperature dependence (Fig. 2c): it decreases with increasing temperature. At temperatures above 200 K, the signal becomes too weak and could not be reliably recorded for analysis. Therefore, we focus our discussion on the temperature range of 5 - 180 K. To gain a quantitative understanding of the doping-induced unpaired electrons, we determine their magnetic susceptibility  $\chi_{\rm g}$  by double integration of the ESR spectra using a CuSO<sub>4</sub> crystal as the spin concentration standard (see Methods), and the resultant temperature-dependent magnetic susceptibility is shown in Fig. 3a. The fact that the magnetic susceptibility decreases with increasing temperature excludes the possibility of conduction electron-related Pauli spin susceptibility, which is independent of temperature.<sup>57</sup> Plotting the magnetic susceptibility against the inverse temperature 1/T (Fig. 3b) reveals a Curie law behavior:  $\chi_g = C/T$ , where C is the Curie constant. Similar temperaturedependent ESR signals can be observed for SWCNTs functionalized by other types of diazonium salts. Together shown in Fig. 3a and 3b are the temperature-dependent magnetic susceptibility of SWCNTs functionalized by dichlorobenzenediazonium tetrafluoroborate (Cl<sub>2</sub>-Dz) and a similar Curie law behavior can also be observed. For the NO<sub>2</sub>-Dz- and Cl<sub>2</sub>-Dz-doped SWCNTs, Curie constants of 6.10×10<sup>-7</sup> and 6.51×10<sup>-7</sup> emuK/g can be obtained, respectively. The common behavior shared by the different types of diazonium salt-doped SWCNTs reveals that the spin properties are

defined by the bonding between the diazonium salt and the SWCNT sidewall rather than the specific alkyl group, *e.g.* NO<sub>2</sub>-C<sub>6</sub>H<sub>4</sub>- and Cl<sub>2</sub>-C<sub>6</sub>H<sub>3</sub>- in Fig. 3.

From the Curie constant, we can further derive the corresponding spin concentrations using equation<sup>47</sup>  $C = \frac{\mu_B^2 N}{k_B}$ , in which  $\mu_B$  is the Bohr magneton, N is the number of spins, and  $k_B$  represents the Boltzmann constant. We obtain spin concentrations of  $5.52 \times 10^{14}$  and  $5.66 \times 10^{14}$  spins/cm<sup>3</sup> for NO<sub>2</sub>-Dz- and Cl<sub>2</sub>-Dz-doped SWCNTs, respectively. This bulk spin concentration translates into an average of around 8 spins per 100 nm tube based on our estimation of the SWCNT concentrations in the samples (see Supporting Information S2 for details). In order to find

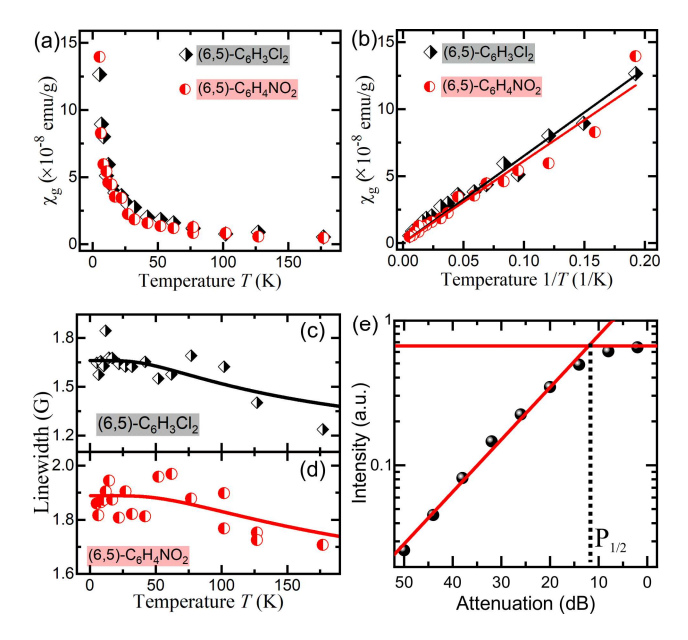


Figure 3. (a, b) Mass spin susceptibility  $\chi_g$  plotted as a function of temperature T(a) and inverse temperature 1/T (b) for NO<sub>2</sub>-Dz- (dots) and Cl<sub>2</sub>-Dz-doped (diamonds) SWCNTs. The lines in (b) are Curie-law fits to the spin susceptibility. (c, d) Temperature-dependent linewidths of the ESR signals for the NO<sub>2</sub>-Dz- (d) and Cl<sub>2</sub>-Dz-doped (c) SWCNTs, together with their fitting curves using equation (2). (e) Microwave power-dependent ESR saturation data (dots) of the NO<sub>2</sub>-Dz-doped SWCNTs at 10 K. The unattenuated maximum output power is 0.2 W.

correlations between the origins of the spins and the  $sp^3$  quantum defects, we also estimate the defect density, which is found to be around 6 defects per 100 nm tube (Supporting Information S2). In this study, the quantum defect concentration is deliberately kept low by our controlled doping method to prevent any photoluminescence quenching caused by over-doping.<sup>6</sup> The reasonable agreement between the spin and defect densities further unveils the quantum defectrelated origin of the spins. The low spin concentration indicates that they are most likely isolated from each other and no exchange interactions should be expected, considering that the wave functions of defect spins typically only spread over a few hexagonal cells.<sup>50</sup> This is consistent with the observed Curie law behavior in Fig. 3a and 3b, which are characteristic of isolated and localized spins. Moreover, by varying the functionalization time, we prepare a set of chemically functionalized SWCNTs with different quantum defect densities and study their ESR spectra (Supporting Information S3). Using the method described above, we are able to derive the spin densities at the different defect concentrations and a good agreement is observed between the two (Fig. S2). This finding indicates the correlation between the quantum defects and the observed spins.

To further confirm these conclusions, we perform density functional theory (DFT) calculations of the pristine and functionalized SWCNTs (see Methods for descriptions of the calculation details). Fig. 4a shows the predicted band structure of pristine (6,5)-SWCNTs and in comparison, the band structure of the NO<sub>2</sub>-Dz-doped SWCNTs is shown in Fig. 4b within the local density approximation. The predicted band gap for the pristine SWCNTs is 0.94 eV, agreeing well with previous DFT calculations,<sup>58</sup> although a slight underestimation compared to experimental results is expected at this level of theory.<sup>59</sup> The predicted Kohn-Sham orbital densities associated with the conduction (marked as 1 in Fig. 4a) and valence bands (marked as 2 in Fig. 4a) at the Γ-point are

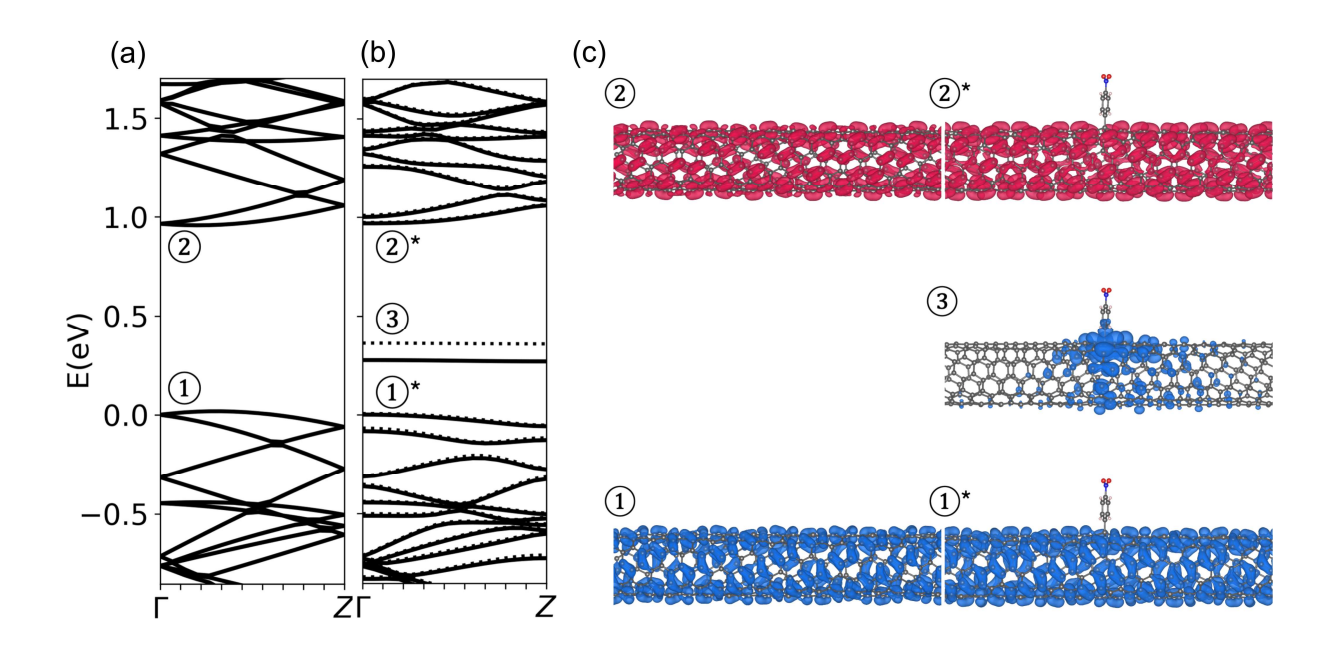


Figure 4. (a, b) Calculated bandstructure of a pristine (6,5)-SWCNT (a) and a NO<sub>2</sub>-Dz-doped SWCNT (b). The zero is defined as the valence band energy at  $\Gamma$ . (c) Plots of the charge densities associated with the selected orbitals labeled as  $(1, 2; 1^*, 2^*, 3)$  on the bandstructure in (a) and (b).

shown in Fig. 4c (left) for the pristine SWCNTs. The orbitals are formed as a linear combination of carbon p-orbitals, and the resultant electron densities are evenly distributed over the entire tube length. The diazonium chemical functionalization leads to an occupied spin up mid-gap state at 0.30 eV above the valence band maximum and an unoccupied spin down state at 0.40 eV above the valence band maximum, as shown in Fig. 4b (marked as 3). While the Kohn-Sham orbital densities of the conduction and valence bands in the functionalized SWCNTs remain delocalized (Fig. 4c, right, 1 and 2), the charge density of the mid-gap state associated with the  $sp^3$  quantum defects is highly localized around the defect site (Fig. 4c, right, 3). The spin density is also localized on the occupied mid-gap orbital. These findings further corroborate our conclusion that the observed spins, which are localized and isolated, are correlated to the  $sp^3$  quantum defects. It has been proposed<sup>60</sup> that during a diazonium functionalization reaction, aryl radials are formed

and react with the SWCNTs, creating *sp*<sup>3</sup>-hybrizied carbon atoms and leaving radicals in the vicinity of the attached phenyl rings. By adding radical scavengers, ferricyanide [Fe(CN)<sub>6</sub>]<sup>3-</sup> ions to the functionalized SWCNT solutions, we observe a direct quenching of their ESR signals (Fig. S3), which indicates the existence of stable radicals in the functionalized SWCNTs. The high stability of the radicals in the quantum defects might be related to the electronic structures of the SWCNTs,<sup>61, 62</sup> although the detailed chemistry merits further thorough investigation. Based on these factors, we tend to assign the localized spins observed in our study to radicals induced by diazonium salt functionalization.

Having identified the origin of the detected spins, we further interrogate the lineshape of the ESR response. ESR spectroscopy measures the magnetic field (H) derivative of the rf power absorbed (P) by the samples. The observed signals follow a Dysonian lineshape:<sup>63</sup>

$$\frac{dP}{dH} = \frac{d}{dH} \left( \frac{\Delta H + \alpha (H - H_0)}{(H - H_0)^2 + \Delta H^2} + \frac{\Delta H + \alpha (H + H_0)}{(H + H_0)^2 + \Delta H^2} \right) \tag{1}$$

where  $H_0$  is the resonance field,  $\Delta H$  is the linewidth, and  $\alpha$  is the asymmetry parameter which represents the ratio between dispersion and absorption. In our case, the rather symmetric lineshape gives rise to  $\alpha$  values between 0 and 0.1, indicating a low admixture of dispersion due to the isolated, localized spins. Fitting the ESR signals with the Dysonian function also allows us to derive their linewidths  $\Delta H$ . Fig. 3c and 3d show the temperature-dependent linewidths of the functionalized SWCNTs. For both types of the functionalized samples, their linewidths remain below 2 G which, as far as we know, is one of the smallest values reported so far for CNTs. <sup>43, 44, 47, 48</sup> The linewidths show negligible temperature dependence at low temperatures, but decrease slightly when the temperature is raised to above 100 K. This weak temperature dependence in the observed linewidth has also been observed for irradiation-induced defects in SWCNTs, <sup>44</sup> and is

consistent with our conclusion above that the doping-introduced spins are highly localized, even at temperatures as high as 100 K. This is in stark contrast to the drastic motional narrowing observed for unbound or shallowly bound spin species,<sup>47</sup> the linewidth of which reduces tremendously with temperature due to the increased charge carrier mobility at higher temperatures and hence their lower probability to dwell at dephasing centers. To describe the temperature-dependent linewidth changes, we adapt a model that describes thermal-induced spin motion caused by phonon-activated spin hopping:<sup>47, 48</sup>

$$\Delta H = \Delta H_0 + \frac{A}{\Delta E \times \left[1 + \cot\left(\frac{\Delta E}{2k_B T}\right)\right]}$$
 (2)

Here,  $\Delta H_0$  is the high-T limit of the linewidth, A a temperature-independent constant, and  $\Delta E$  the activation energy for moving the spins out of potential traps. Fitting of the temperature-dependent linewidths using equation (2) yields the detrapping energies of the localized spins (Fig. 3c and 3d, curves), which are estimated to be 17.3 meV and 12.5 meV for the NO<sub>2</sub>-Dz- and Cl<sub>2</sub>-Dz-doped SWCNTs, respectively. These large detrapping energies explain the weak temperature-dependence of the linewidths observed in Fig. 3c and 3d.

More significantly, from the high-T linewidth limit  $\Delta H_0$ , which are estimated to be 1.41 and 1.05 G for the NO<sub>2</sub>-Dz- and Cl<sub>2</sub>-Dz-doped SWCNTs, respectively, we can derive the spin dephasing time  $T_2$  using the following relation:<sup>64</sup>  $T_2 = \hbar/(g\mu_B\Delta H_0)$ . Utilizing the g-factor and  $\Delta H_0$  values we obtained from the ESR signals, spin dephasing time  $T_2$  of 40.3 ns and 53.9 ns can be obtained for the NO<sub>2</sub>-Dz- and Cl<sub>2</sub>-Dz-doped SWCNTs, respectively. These are the spin dephasing times  $T_2$  at high temperatures provided that the thermal-induced spin motion model described in equation (2) is still valid at such high temperatures. These spin dephasing times are considerably longer

than those reported previously,  $^{47, 65, 66}$  in agreement with the narrow linewidths of our samples. Analyzing the potential reasons, we believe that they are two-fold: the purification and chirality-sorting processes remove the majority of the catalyst particles and carbon impurities that may serve as dephasing centers; the diazonium doping method allows a relatively good control over the defect and spin concentrations, thus minimizing dipolar interactions among the spins. Despite the encouraging  $T_2$  value observed here, it is still below expectations for practical use. For example, the current state-of-the-art lower bound for signal processing times in quantum electronic devices is around 100 ns.  $^{67}$  However, procedures such as reducing the percentage of  $^{13}$ C isotope during growth for reduced hyperfine coupling may help further increase the spin dephasing time.

Due to the limited defect and spin concentrations we are able to achieve without causing permanent photoluminescence quenching to the SWCNTs, direct investigation of the spin relaxation times utilizing time-resolved ESR methods is challenging due to their lower signal-to-noise ratios compared to cw ESR measurements. However, continuous-wave power-saturation measurements, analysed with the method developed by Castner *et al.*,<sup>68</sup> provide an alternative approach for estimating the spin-lattice relaxation time  $T_1$ .<sup>69, 70</sup> Fig. 3e shows representative power-dependent ESR intensities of the NO<sub>2</sub>-Dz-doped SWCNTs at 10 K. The signal strength increases with power until it reaches a plateau. The onset of the power-saturation behaviour, represented by characteristic parameters  $P_{1/2}$  and  $H_{1/2}$ , is determined by the spin relaxation dynamics. Using Castner *et al.*'s approach, we estimate the value of  $P_{1/2}$ , *i.e.* the intersection of the two red lines in Fig. 3e, to be around 12.1 dB (12.3 mW), and  $H_{1/2}$  to be around 0.19 G. Using the correlation<sup>68,71</sup> value, we determine the spin-lattice relaxation time  $T_1$  to be around 9.1 µs, close to previously reported values.<sup>48</sup>

### **CONCLUSION**

We study spin properties of SWCNTs functionalized by diazonium salts utilizing temperature- and power-dependent ESR measurements. In stark contrast to pristine SWCNTs, which exhibit minimal ESR signals, those functionalized with  $sp^3$  defects show apparent narrow ESR lines. Our analysis of the temperature-dependent magnetic susceptibility in combination with the spin density estimation infers the creation of sparse, localized spins in the functionalized SWCNTs, which is further confirmed by our DFT calculations. From the temperature-dependent linewidth analysis and power-saturation measurements, we estimate the spin dephasing time  $T_2$  and spin-lattice relaxation time  $T_1$  to be around 40 ns and 9  $\mu$ s, respectively. The dephasing time, although still below the expected values for practical applications, can be improved substantially by suppressing paramagnetic defects<sup>72</sup> and isotope engineering<sup>73</sup> to reduce nuclear spins. The observed spin states at the defect sites, together with the intriguing optical properties of the  $sp^3$  quantum defects,  $^{2}$ ,  $^{6}$ ,  $^{13}$ ,  $^{14}$ ,  $^{20}$ ,  $^{37}$  may enable the application of SWCNTs in spin-based quantum devices. Further studies of the chemically functionalized SWCNTs using optically detected magnetic resonance may provide more insights about the triplet states and the related spin states in the quantum defects.  $^{74}$ 

## **METHODS**

Chirality sorting and chemical functionalization of the single-walled carbon nanotubes. The SWCNT samples were purified and chemically functionalized following previously published methods<sup>2, 75, 76</sup> with some modifications. In brief, (6,5)-enriched SWCNT samples (CoMoCAT SG65i) were dispersed in 1 % wt/v sodium deoxycholate (DOC) solution by tip sonication for 90 minutes while cooled in an ice bath. Catalyst particles, amorphous carbon and CNT bundles were removed by ultracentrifugation for 2 hours at the speed of 39191 g at room temperature. The

supernatants were used for chirality sorting following the two-step phase separation method. The resultant single-chirality (6,5)-SWCNTs were then transferred into 1 % wt/v sodium dodecyl sulfate (SDS) solution by pressure filtration. In order to chemically functionalize the SWCNTs with diazonium salts, appropriate amounts of the diazonium salt solutions were added to the SWCNT solutions. The reaction progress was monitored by measuring the PL spectra of the solutions. Once the designated doping levels were achieved, the reactions were quenched by the addition of concentrated DOC solutions. The functionalized SWCNTs were then transferred back into 1 % wt/v DOC solution using pressure filtration. To ensure that the excess unreacted diazonium salts were removed, the SWCNT dispersions were repeatedly washed by pressure filtration through a 100 kDa cellulose membrane using 1% wt/v DOC solution as elute for 5 to 6 times.

Electron spin resonance measurements. The temperature- and power-dependent ESR measurements were performed using an ELEXSYS-II E500 X-Band cw spectrometer equipped with a TE<sub>102</sub> rectangular ESR resonator (Bruker ER 4102ST), operating at a microwave frequency of 9.5 GHz (Bruker Biospin, Rheinstetten, Germany). A continuous flow Helium cryostat (ICE Oxford, UK) and an ITC (Oxford Instruments, UK) were used to control the temperature. For the measurements, the SWCNT samples were transferred into quartz tubes in a nitrogen glove box and sealed. Afterwards, the sealed samples were rapidly frozen in liquid nitrogen and loaded into the pre-cooled sample chamber. To calibrate the spin concentrations in the measured SWCNT samples, a CuSO<sub>4</sub> single crystal with a known number of spins was used as a standard.

Electronic structure and spin state calculation. The electronic structures and spin properties of the (6,5)-SWCNTs with and without the dopants were calculated using the local spin density functional approximation (LSDA)<sup>77</sup> calculated within the VASP package.<sup>78</sup> Core electrons and

nuclei were described by the projector-augmented wave method (PAW). 79 Scalar relativistic effects were included in the PAW potential, and spin-orbit coupling (SOC) were added perturbatively using the zero-order regular approximation<sup>80</sup> through the second-variation method.<sup>81</sup> All self-consistent calculations were performed with a plane wave cutoff energy of 400 eV, and a k = 0 ( $\Gamma$ )-centered k-point mesh of 1x1x2. The choice of k-mesh converged the total energy to less than 0.005 meV/atom. Each self-consistent cycle electronic energy was converged to below 1x10<sup>-6</sup> eV. For the pristine SWCNTs, the structure was optimized such that forces between atoms were smaller than 0.01 eV/Å and total energy change was less than  $1 \times 10^{-4} \text{ eV}$ . 10 Å of vacuum were added around the tube to isolate it from its periodic images. The predicted lattice vectors were (19.92, 19.92, 40.45) Å for the pristine and (32.37, 19.92, 40.45) Å for the functionalized SWCNTs. The predicted lattice vector length of 40.45 Å along the nanotube direction is in good agreement with a tight binding analysis<sup>82</sup> and previous DFT calculations.<sup>58</sup> Band structures were calculated non-self-consistently on a 1 x 1 x 16 k-point mesh. For the doped structure, the lattice vectors of the SWCNTs were fixed and the atoms allowed to relax in the presence of the dopants with forces converged to less than 0.01 eV/Å. The magnetic moment was optimized and determined to be 1 Bohr magneton.

#### ASSOCIATED CONTENT

# **Supporting Information.**

The following files are available free of charge:

ESR spectrum of diazonium salts; detailed calculation method of the spin and quantum defect

densities; correlation between the defect and spin densities; influence of radical scavengers.

**AUTHOR INFORMATION** 

**Corresponding Author** 

\*Email: xuedan.ma@anl.gov

**Notes** 

The authors declare no competing final interest.

ACKNOWLEDGMENT

We acknowledge support from the National Science Foundation DMR Program under the award

no. DMR-1905990. Use of the Center for Nanoscale Materials, an Office of Science user facility,

was supported by the U.S. Department of Energy, Office of Science, Office of Basic Energy

Sciences, under Contract No. DE-AC02-06CH11357. We thank Tijana Rajh for insightful

discussions about the results. The ESR measurements were supported by the U.S. Department of

Energy, Office of Science, Office of Basic Energy Sciences, Division of Chemical Sciences,

Geosciences, and Biosciences under contract number DE-AC02-06CH11357. This research used

resources of the National Energy Research Scientific Computing Center (NERSC), a U.S.

Department of Energy Office of Science User Facility operated under Contract No. DE-AC02-

05CH11231.

17

#### **REFERENCES**

- 1. Ghosh, S.; Bachilo, S. M.; Simonette, R. A.; Beckingham, K. M.; Weisman, R. B. Oxygen Doping Modifies Near-Infrared Band Gaps in Fluorescent Single-Walled Carbon Nanotubes. *Science* **2010**, *330*, 1656-1659.
- 2. Piao, Y.; Meany, B.; Powell, L. R.; Valley, N.; Kwon, H.; Schatz, G. C.; Wang, Y. . Brightening of Carbon Nanotube Photoluminescence through the Incorporation of *sp*<sup>3</sup> Defects. *Nat. Chem.* **2013**, *5*, 840-845.
- 3. Ma, X.; Baldwin, J. K. S.; Hartmann, N. F.; Doorn, S. K.; Htoon, H. Solid-State Approach for Fabrication of Photostable, Oxygen-Doped Carbon Nanotubes. *Adv. Funct. Mater.* **2015**, *25*, 6157-6164.
- 4. Chiu, C. F.; Saidi, W. A.; Kagan, V. E.; Star, A. Defect-Induced Near-Infrared Photoluminescence of Single-Walled Carbon Nanotubes Treated with Polyunsaturated Fatty Acids. *J. Am. Chem. Soc.* **2017**, *139*, 4859-4865.
- 5. Ma, X.; Adamska, L.; Yamaguchi, H.; Yalcin, S. E.; Tretiak, S.; Doorn, S. K.; Htoon, H. Electronic Structure and Chemical Nature of Oxygen Dopant States in Carbon Nanotubes. *ACS Nano* **2014**, *8*, 10782-10789.
- 6. Sykes, M. E.; Kim, M.; Wu, X.; Wiederrecht, G. P.; Peng, L.; Wang, Y.; Gosztola, D. J.; Ma, X. Ultrafast Exciton Trapping at *sp*<sup>3</sup> Quantum Defects in Carbon Nanotubes. *ACS Nano* **2019**, *13*, 13264-13270.
- 7. Danné, N.; Kim, M.; Godin, A. G.; Kwon, H.; Gao, Z.; Wu, X.; Hartmann, N. F.; Doorn, S. K.; Lounis, B.; Wang, Y.; Cognet, L. Ultrashort Carbon Nanotubes That Fluoresce Brightly in the Near-Infrared. *ACS Nano* **2018**, *12*, 6059-6065.
- 8. Iwamura, M.; Akizuki, N.; Miyauchi, Y.; Mouri, S.; Shaver, J.; Gao, Z.; Cognet, L.; Lounis, B.; Matsuda, K. Nonlinear Photoluminescence Spectroscopy of Carbon Nanotubes with Localized Exciton States. *ACS Nano* **2014**, *8*, 11254-11260.
- 9. Miyauchi, Y.; Iwamura, M.; Mouri, S.; Kawazoe, T.; Ohtsu, M.; Matsuda, K. Brightening of Excitons in Carbon Nanotubes on Dimensionality Modification. *Nat. Photon.* **2013**, *7*, 715-719. 10. Ma, X.; Roslyak, O.; Duque, J. G.; Pang, X.; Doorn, S. K.; Piryatinski, A.; Dunlap, D. H.; Htoon, H. Influences of Exciton Diffusion and Exciton-Exciton Annihilation on Photon Emission Statistics of Carbon Nanotubes. *Phys. Rev. Lett.* **2015**, *115*, 017401.

- 11. Högele, A.; Galland, C.; Winger, M.; Imamoğlu, A. Photon Antibunching in the Photoluminescence Spectra of a Single Carbon Nanotube. *Phys. Rev. Lett.* **2008**, *100*, 217401.
- 12. Ma, X.; Hartmann, N. F.; Velizhanin, K. A.; Baldwin, J. K. S.; Adamska, L.; Tretiak, S.; Doorn, S. K.; Htoon, H. Multi-Exciton Emission from Solitary Dopant States of Carbon Nanotubes. *Nanoscale* **2017**, *9*, 16143-16148.
- 13. Ma, X.; Hartmann, N. F.; Baldwin, J. K. S.; Doorn, S. K.; Htoon, H. Room-Temperature Single-Photon Generation from Solitary Dopants of Carbon Nanotubes. *Nat. Nanotechnol.* **2015**, *10*, 671-675.
- 14. He, X.; Hartmann, N. F.; Ma, X.; Kim, Y.; Ihly, R.; Blackburn, J. L.; Gao, W.; Kono, J.; Yomogida, Y.; Hirano, A.; Tanaka, T.; Karaura, H.; Htoon, H.; Doorn, S. K. Tunable Room-Temperature Single-Photon Emission at Telecom Wavelengths from *sp*<sup>3</sup> Defects in Carbon Nanotubes. *Nat. Photon.* **2017**, *11*, 577-582.
- 15. Saha, A.; Gifford, B. J.; He, X.; Ao, G.; Zheng, M.; Kataura, H.; Htoon, H.; Kilina, S.; Tretiak, S.; Doorn, S. K. Narrow-Band Single-Photon Emission through Selective Aryl Functionalization of Zigzag Carbon Nanotubes. *Nat. Chem.* **2018**, *10*, 1089-1095.
- 16. Pyatkov, F.; Fütterling, V.; Khasminskaya, S.; Flavel, B. S.; Hennrich, F.; Kappes, M. M; Krupke, R.; Pernice, W. H. P. Cavity-Enhanced Light Emission from Electrically Driven Carbon Nanotubes. *Nat. Photon.* **2016**, *10*, 420-427.
- 17. Jeantet, A.; Chassagneux, Y.; Raynaud, C.; Roussignol, Ph.; Lauret, J. S.; Besga, B.; Estève, J.; Reichel, J.; Voisin, C. Widely Tunable Single-Photon Source from a Carbon Nanotube in the Purcell Regime. *Phys. Rev. Lett.* **2016**, *116*, 247402.
- 18. Ma, X.; Htoon, H. Tailoring the Photophysical Properties of Carbon Nanotubes by Photonic Nanostructures. *Mod. Phys. Rev. B* **2015**, *29*, 1530004.
- 19. Ma, X.; James, A. R.; Hartmann, N. F.; Baldwin, J. K.; Dominguez, J.; SInclair, M. B.; Luk, T. S.; Wolf, O.; Liu, S.; Doorn, S. K.; Htoon, H.; Brener, I. Solitary Oxygen Dopant Emission from Carbon Nanotubes Modified by Dielectric Metasurfaces. *ACS Nano* **2017**, *11*, 6431-6439. 20. Ishii, A.; He, X.; Hartmann, N. F.; Machiya, H.; Htoon, H.; Doorn, S. K.; Kato, Y. K. Enhanced Single-Photon Emission from Carbon-Nanotube Dopant States Coupled to Silicon Microcavities. *Nano Lett.* **2018**, *18*, 3873-3878.

- 21. Luo, Y.; Ahmadi, E. D.; Shayan, K.; Ma, Y.; Mistry, K. S.; Zhang, C.; Hone, J.; Blackburn, J. L.; Strauf, S. Purcell-Enhanced Quantum Yield from Carbon Nanotube Excitons Coupled to
- Plasmonic Nanocavities. Nat. Commun. 2017, 8, 1413.
- 22. Graf, A.; Tropf, L.; Zakharko, Y.; Zaumseil, J.; Gather, M. C. Near-Infrared Exciton-Polaritons in Strongly Coupled Single-Walled Carbon Nanotube Microcavities. *Nat. Commun.* **2016,** *7*, 13078.
- 23. Nowack, K. C.; Koppens, F. H. L.; Nazarov, V.; Vandersypen, L. M. K. Coherent Control of a Single Electron Spin with Electric Fields. *Science* **2007**, *318*, 1430-1433.
- 24. Laird, E. A.; Pei, F.; Kouwenhoven, L. P. A Valley–Spin Qubit in a Carbon Nanotube. *Nat. Nanotechnol.* **2013**, *8*, 565-568.
- 25. Kuermmeth, F.; Churchill, H. O. H.; Herring, P. K.; Marcus, C. M. Carbon Nanotubes for Coherent Spintronics. *Mater. Today* **2010**, *13*, 18-26.
- 26. Laird, E. A.; Kuemmeth, F.; Steele, G. A.; Grove-Rasmussen, K.; Nygård, J.; Flensberg, K.; Kouwenhoven, L. P. Quantum Transport in Carbon Nanotubes. *Rev. Mod. Phys.* **2015**, *87*, 703.
- 27. Fischer, J.; Trauzettel, B.; Loss, D. Hyperfine Interaction and Electron-Spin Decoherence in Graphene and Carbon Nanotube Quantum Dots. *Phys. Rev. B* **2009**, *80*, 155401.
- 28. Semenov, Y. G.; Kim, K. W.; Iafrate, G. J. Electron Spin Relaxation in Semiconducting Carbon Nanotubes: The Role of Hyperfine Interaction. *Phys. Rev. B* **2007**, *75*, 045429.
- 29. Pei, F.; Laird, E. A.; Steele, G. A.; Kouwenhoven, L. P. Valley–Spin Blockade and Spin Resonance in Carbon Nanotubes. *Nat. Nanotechnol.* **2012,** *7*, 630-634.
- 30. Pályi, A.; Struck, P. R.; Rudner, M.; Flensberg, K.; Burkard, G. Spin-Orbit-Induced Strong Coupling of a Single Spin to a Nanomechanical Resonator. *Phys. Rev. Lett.* **2012**, *108*, 206811.
- 31. Struck, P. R.; Wang, H.; Burkard, G. Nanomechanical Readout of a Single Spin. *Phys. Rev.* B **2014**, *89*, 045404.
- 32. Viennot, J. J.; Dartiailh, M. C.; Cottet, A.; Kontos, T. Coherent Coupling of a Single Spin to Microwave Cavity Photons. *Science* **2015**, *349*, 408-411.
- 33. Cubaynes, T.; Delbecq, M. R.; Dartiailh, M. C.; Assouly R.; Desjardins, M. M; Contamin, L.
- C.; Bruhat, L. E.; Leghtas, Z.; Mallet, F.; Cottet, A.; Kontos, T. Highly Coherent Spin States in Carbon Nanotubes Coupled to Cavity Photons. *Npj Quantum Inf.* **2019**, *5*, 47.
- 34. Galland, C.; Imamoğlu, A. All-Optical Manipulation of Electron Spins in Carbon-Nanotube Quantum Dots. *Phys. Rev. Lett.* **2008**, *101*, 157404.

- 35. Santos, S. M.; Yuma, B.; Berciaud, S.; Shaver, J.; Gallart, M.; Gilliot, P.; Cognet, L.; Lounis, B. All-Optical Trion Generation in Single-Walled Carbon Nanotubes. *Phys. Rev. Lett.* **2011**, *107*, 187401.
- 36. Deilmann, T.; Drüppel, M.; Rohlfing, M. Three-Particle Correlation from a Many-Body Perspective: Trions in a Carbon Nanotube. *Phys. Rev. Lett.* **2016**, *116*, 196804.
- 37. Hartmann, N. F.; Velizhanin, K. A.; Haroz, E. H.; Kim, M.; Ma, X.; Wang, Y.; Htoon, H.; Doorn, S. K. Photoluminescence Dynamics of Aryl *sp*<sup>3</sup> Defect States in Single-Walled Carbon Nanotubes. *ACS Nano* **2016**, *10*, 8355-8365.
- 38. Chiesa, M.; Giamello, E.; Che, M. EPR Characterization and Reactivity of Surface-Localized Inorganic Radicals and Radical Ions. *Chem. Rev.* **2010**, *110*, 1320-1347.
- 39. Panchenko, A.; Dilger, H.; Möller, E.;Sixt, T.; Roduner, E. *In Situ* EPR Investigation of Polymer Electrolyte Membrane Degradation in Fuel Cell Applications. *J. Power Souces* **2004**, *127*, 325-330.
- 40. Krzystek, J.; Ozarowski, A.; Telser, J. Multi-Frequency, High-Field EPR as a Powerful Tool to Accurately Determine Zero-Field Splitting in High-Spin Transition Metal Coordination Complexes. *Coord. Chem. Rev.* **2006**, *250*, 2308-2324.
- 41. Kuemmeth, F.; Ilani, S.; Ralph, D. C.; McEuen, P. L. Coupling of Spin and Orbital Motion of Electrons in Carbon Nanotubes. *Nature* **2008**, *452*, 448-452.
- 42. Kosaka, M.; Ebbesen, T. W.; Hiura, H.; Tanigaki, K. Electron Spin Resonance of Carbon Nanotubes. *Chem. Phys. Lett.* **1994,** *225*, 161-164.
- 43. Claye, A. S.; Nemes, N. M.; Jánossy, A.; Fischer, J. E. Structure and Electronic Properties of Potassium-Doped Single-Wall Carbon Nanotubes. *Phys. Rev. B* **2000**, *62*, R4845-R4848.
- 44. Salvetat, J.-P.; Fehér, T.; L'Huillier, C.; Beuneu, F.; Forró, L. Anomalous Electron Spin Resonance Behavior of Single-Walled Carbon Nanotubes. *Phys. Rev. B* **2005**, *72*, 075440.
- 45. Náfrádi, B.; Nemes, N. M.; Fehér, T.; Forró, L.; Kim, Y.; Fischer, J. E.; Luzzi, D. E.; Simon,
- F.; Kuzmany, H. Electron Spin Resonance of Single-Walled Carbon Nanotubes and Related Structures. *Phys. Status Solidi B* **2006**, *243*, 3106-3110.
- 46. Zaka, M.; Ito, Y.; Wang, H.; Yan, W.; Robertson, A.; Wu, Y. A.; Rümmeli, M. H.; Staunton, D.; Hashimoto, T.; Morton, J. J. L.; Ardavan, A.; Briggs, G. A. D.; Warner, J. H. Electron Paramagnetic Resonance Investigation of Purified Catalyst-Free Single-Walled Carbon Nanotubes. *ACS Nano* **2010**, *4*, 7708-7716.

- 47. Rice, W. D.; Weber, R. T.; Leonard, A. D.; Tour, J. M.; Nikolaev, P.; Arepalli, S.; Berka, V.; Tsai, A.-L.; Kono, J. Enhancement of the Electron Spin Resonance of Single-Walled Carbon Nanotubes by Oxygen Removal. *ACS Nano* **2012**, *6*, 2165-2173.
- 48. Rice, W. D.; Weber, R. T.; Nikolaev, P.; Arepalli, S.; Berka, V.; Tsai, A.-L.; Kono, J. Spin Relaxation Times of Single-Wall Carbon Nanotubes. *Phys. Rev. B* **2013**, *88*, 041401(R).
- 49. Ferrer-Anglada, N.; Monge, A. A.; Roth, S. Electron Spin Resonance on Single-Walled Carbon Nanotubes Obtained from Different Sources. *Phys. Status Solidi B* **2010**, *247*, 2823-2826.
- 50. Havlicek, M.; Jantsch, W.; Wilamowski, Z.; Yanagi, K.; Kataura, H.; Rümmeli, M. H.; Malissa, H.; Tyryshkin, A.; Lyon, S.; Chernov, A.; Kuzmany, H. Indirect Exchange Interaction in Fully Metal-Semiconductor Separated Single-Walled Carbon Nanotubes Revealed by Electron Spin Resonance. *Phys. Rev. B* **2012**, *86*, 045402.
- 51. Bockrath, M.; Cobden, D. H.; Lu, J.; Rinzler, A. G.; Smalley, R. E.; Balents, L.; McEuen, P. L. Luttinger-Liquid Behaviour in Carbon Nanotubes. *Nature* **1999**, *397*, 598-601.
- 52. Ishii, H.; Kataura, H.; Shiozawa, H.; Yoshioka, H.; Otsubo, H.; Takayama, Y.; Miyahara, T.; Suzuki, S.; Achiba, Y.; Nakatake, M.; Narimura, T.; Higashiguchi, M.; Shimada, K.; Namatame, H.; Taniguchi, M. Direct Observation of Tomonaga–Luttinger-Liquid State in Carbon Nanotubes at Low Temperatures. *Nature* **2003**, *426*, 540-544.
- 53. Dóra, B.; Gulácsi, M.; Koltai, J.; Zólyomi, V.; Kürti, J.; Simon, F. Electron Spin Resonance Signal of Luttinger Liquids and Single-Wall Carbon Nanotubes. *Phys. Rev. Lett.* **2008**, *101*, 106408.
- 54. Kuemmeth, F.; Ilani, S.; Ralph, D. C.; McEuen, P. L. Coupling of Spin and Orbital Motion of Electrons in Carbon Nanotubes. *Nature* **2008**, *2008*, 448-452.
- 55. Huertas-Hernando, D.; Guinea, F.; Brataas, A. Spin-Orbit Coupling in Curved Graphene, Fullerenes, Nanotubes, and Nanotube Caps. *Phys. Rev. B* **2006**, *74*, 155426.
- 56. Likodimos, V.; Glenis, S.; Guskos, N.; Lin, C. L. Antiferromagnetic Behavior in Single-Wall Carbon Nanotubes. *Phys. Rev. B* **2007**, *76*, 075420.
- 57. Kittel, C. Introduction to Solid State Physics; Wiley: New York, 1996.
- 58. Correa, J. D.; Orellana, W. Light-Harvesting Efficiency of a (6,5) Carbon Nanotube Functionalized with a Free-Base Tetraphenylporphyrin: Density Functional Theory Calculations. *J. Appl. Phys.* **2013**, *113*, 174305.

- 59. Perdew, J. P. Density Functional Theory and the Band Gap Problem. *Int. J. Quantum Chem.* **1985,** *28*, 497-523.
- 60. Bahr, J. L.; Yang, J.; Kosynkin, D. V.; Bronikowski, M. J.; Smalley, R. E.; Tour, J. M. Functionalization of Carbon Nanotubes by Electrochemical Reduction of Aryl Diazonium Salts: A Bucky Paper Electrode. *J. Am. Chem. Soc.* **2001**, *123*, 6536-6542.
- 61. Schmidt, G.; Gallon, S.; Esnouf, S.; Bourgoin, J.-P.; Chenevier, P. Mechanism of the Coupling of Diazonium to Single-Walled Carbon Nanotubes and Its Consequences. *Chem. Eur. J* **2009,** *15*, 2101-2110.
- 62. Sheka, E. F. Spin Chemistry of  $sp^2$  Nanocarbons. 2019, 1900.06402. arXiv. https://arxiv.org/abs/1909.06402 (September 13, 2019).
- 63. Joshi, J. P.; Gupta, R.; Sood, A. K.; Bhat, S. V.; Raju, A. R.; Rao, C. N. R. Temperature-Dependent Electron Paramagnetic Resonance Studies of Charge-Ordered Nd<sub>0.5</sub>Ca<sub>0.5</sub>MnO<sub>3</sub>. *Phys. Rev. B* **2001**, *65*, 024410.
- 64. Dyakonov, M. I. *Spin Physics in Semiconductors*, Edition 1; Springer International Publishing: Berlin, 2017.
- 65. Petit, P.; Jouguelet, E.; Fischer, J. E.; Rinzler, A. G.; Smalley, R. E. Electron Spin Resonance and Microwave Resistivity of Single-Wall Carbon Nanotubes. *Phys. Rev. B* **1997**, *56*, 9275-9278.
- 66. Corzilius, B.; Dinse, K.-P..; Hata, K. Single-Wall Carbon Nanotubes and Peapods Investigated by EPR. *Phys. Chem. Chem. Phys.* **2007**, *9*, 6063-6072.
- 67. Colless, J. I.; Mahoney, A. C.; Hornibrook, J. M.; Doherty, A. C.; Lu, H.; Gossard, A. C.; Reilly, D. J. Dispersive Readout of a Few-Electron Double Quantum Dot with Fast rf Gate Sensors. *Phys. Rev. Lett.* **2013**, *110*, 046805.
- 68. Castner, T. G. Saturation of the Paramagnetic Resonance of a V Center. *Phys. Rev.* **1959**, 115, 1506.
- 69. Heinemann, M. D.; von Maydell, K.; Zutz, F.; Kolny-Olesiak, J.; Borchert, H.; Riedel, I.; Parisi, J. Photo-Induced Charge Transfer and Relaxation of Persistent Charge Carriers in Polymer/Nanocrystal Composites for Applications in Hybrid Solar Cells. *Adv. Funct. Mater.* **2009**, *19*, 3788-3795.

- 70. Zoppellaro, G.; Bakandritsos, A.; Tuček, J.; Błoński, P.; Susi, T.; Lazar, P.; Bad'ura, Z.; Steklý, T.; Opletalová, A.; Otyepka, M.; Zbořil, R. Microwave Energy Drives "On–Off–On" Spin-Switch Behavior in Nitrogen-Doped Graphene. *Adv. Mater.* **2019**, *31*, 1902587.
- 71. Sahlin, M.; Gräslund, A.; Ehrenberg, A. Determination of Relaxation Times for a Free Radical from Microwave Saturation Studies. *J. Magn. Reson.* **1969**, *67*, 135-137.
- 72. Isberg, J.; Hammersberg, J.; Johansson, E.; Wikström, T.; Twitchen, D. J.; Whitehead, A. J.; Coe, S. E.; Scarsbrook, G. A. High Carrier Mobility in Single-Crystal Plasma-Deposited Diamond. *Science* **2002**, *297*, 1670-1672.
- 73. Muhonen, J. T.; Dehollain, J. P.; Laucht, A.; Hudson, F. E.; Kalra, R.; Sekiguchi, T.; Itoh, K. M.; Jamieson, D. N.; McCallum, J. C.; Dzurak, A. S.; Morello, A. Storing Quantum Information for 30 Seconds in a Nanoelectronic Device. *Nat. Nanotechnol.* **2014**, *9*, 986-991.
- 74. D. Stich, F. Späth, H. Kraus, A. Sperlich, V. Dyakonov, T. Hertel. Triplet–Triplet Exciton Dynamics in Single-Walled Carbon Nanotubes. *Nat. Photon.* **2014**, *8*, 139-144.
- 75. Khripin, C. Y.; Fagan, J. A.; Zheng, M. Spontaneous Partition of Carbon Nanotubes in Polymer-Modified Aqueous Phases. *J. Am. Chem. Soc.* **2013**, *135*, 6822-6825.
- 76. Subbaiyan, N. K.; Cambré, S.; Parra-Vasquez, A. Nicholas G.; Hároz, E. H.; Doorn, S. K.; Duque, J. G. Role of Surfactants and Salt in Aqueous Two-Phase Separation of Carbon Nanotubes toward Simple Chirality Isolation. *ACS Nano* **2014**, *8*, 1619-1628.
- 77. Ceperley, D. M.; Alder, B. J. Ground State of the Electron Gas by a Stochastic Method. *Phys. Rev. Lett.* **1980**, *45*, 566-569.
- 78. Blöchl, P. E. Projector Augmented-Wave Method. *Phys. Rev. B* **1994**, *50*, 17953-17979.
- 79. Kresse, G.; Joubert, D. From Ultrasoft Pseudopotentials to the Projector Augmented-Wave Method. *Phys. Rev. B* **1999**, *59*, 1758-1775.
- 80. van Lenthe, E.; Baerends, E. J.; Snijders, J. G. Relativistic Regular Two-Component Hamiltonians. *J. Chem. Phys.* **1993**, *99*, 4597.
- 81. Koelling, D. D.; Harmon, B. N. A Technique for Relativistic Spin-Polarised Calculations. *J. Phys. C: Solid State Phys.* **1977**, *10*, 3107-3114.
- 82. Yang, L.; Anantram, M. P.; Han, J.; Lu, J. P. Band-Gap Change of Carbon Nanotubes: Effect of Small Uniaxial and Torsional Strain. *Phys. Rev. B* **1999**, *60*, 13874-13878.

